Desalination and Water Treatment
www.deswater.com

doi: 10.5004/dwt.2022.28121

250 (2022) 148–158
February

Magnesium ion effect in the process of lithium migration in salt lake

Xin Liu[a,b,c,d,†], Yanfang Ma[b,c,d,*], Guojian Liu[e], Shaoji Xiang[d,f], Zhenhua Cui[d,f]

[a]*University of Chinese Academy of Sciences, Beijing 100190, China, email: liuxin192@mails.ucas.ac.cn (X. Liu)*
[b]*Key Laboratory of Comprehensive and Highly Efficient Utilization of Salt Lake Resources, Qinghai Institute of Salt Lakes, Chinese Academy of Sciences, Xining 810008, China, email: mayanfang@isl.ac.cn (Y. Ma)*
[c]*Key Laboratory of Salt Lake Resources Chemistry of Qinghai Province, Xining 810008, China*
[d]*Innovation Academy for Green Manufacture, Chinese Academy of Sciences, Beijing 100190, China, emails: xiangshaoji@163.com (S. Xiang), cuizhenhua@sioc.ac (Z. Cui)*
[e]*Qinghai Salt Lake Magnesium Co., Ltd., Geermu, Qinghai 81099, China, emails: 2298198658@qq.com*
[f]*Key Laboratory of Organofluorine Chemistry, Shanghai Institute of Organic Chemistry, University of Chinese Academy of Sciences, Chinese Academy of Sciences, Shanghai 200032, China*

Received 10 September 2021; Accepted 30 December 2021

ABSTRACT

The Mg/Li ratio is an important factor in the extraction of Li^+ from salt lake brine. Since Mg^{2+} can exist by competing with Li^+ in the carbonate phase, the cost and energy consumption of Li extraction from salt lakes, is directly affected by the ratio. This article considers the influence of different content of Mg^{2+} on Li_2CO_3 crystal in Na^+, Li^+, CO_3^{2-}//H_2O crystallisation system. In the experiment and calculation simulations, the morphology, particle size and purity of Li_2CO_3 crystals under various Mg/Li ratios were studied. We analysed the mechanism of Mg^{2+} in the Li_2CO_3 crystallisation system, and established the governing equation in relation to the Mg^{2+} content and specific surface area. This research provides theoretical guidance for improving the utilisation rate of Li resources and strengthening the Li_2CO_3 crystallisation process in salt lakes.

Keywords: Salt lake; Li_2CO_3; Mg^{2+}; Specific surface area; Adsorption and doping; Density functional theory

1. Introduction

Because of the superior physical and chemical properties of lithium and its compounds, they are widely used in many fields [1]; among them, Li_2CO_3 is a stable and common basic lithium compound, whose thermal stability is lower than other elements in the periodic table Li_2CO_3 is a carbonate, and therefore is difficult to deliquesce in the air. Thus, it is widely used in batteries, glasses, ceramics, medicine and other industries [2–5]. In recent years, with the rapid development of new energy sources in the electric vehicle industry, the demand for Li_2CO_3 has also increased [6,7]. According to the USGS (U.S. Geological Survey), lithium resources in the world primarily mainly include two types: (1) salt lake brine resources, accounting for 72.31% of the total lithium resources, (2) lithium mineral resources, accounting for 20.26% of the total lithium resources. Due to the high cost of extracting lithium from the ore, and the complex and difficult extraction process that is employed causes serious environmental pollution [8,9]. However, the brine lithium resource which has a simple, affordable extraction method is also rich in yield and is thus widely available to bridged the current supply and demand gap for lithium resources [10]. Therefore, the salt lake brine resources have become an important source for lithium resource development and extraction.

* Corresponding author.
† Co-first author.

At present, the extraction and preparation of Li_2CO_3 products using salt lake brine as raw materials is mainly achieved by precipitation [1]. In this method, the salt lake brine is processed to obtain Li-rich brine and then further subjected to the process of obtaining extraction of Li_2CO_3. However, due to the complex solvent components in the brine, lithium compounds often coexist with alkali metal and alkaline earth metal ions during the extraction process; additionally, the complex solvent components in the brine greatly increases the difficulty of lithium salt separation and extraction [12,13]. The Li-rich solution obtained from brine contains impurities such as Na^+, K^+, Mg^{2+}, SO_4^{2-}, etc; these impurity ions would combine with Li_2CO_3 crystals via adsorption, inclusion, and wrapping processes [14]. These impurities affect the recycling of lithium resources in brine [15], the extraction and preparation of high-purity Li_2CO_3 products [16], and the production and application of Li^+ batteries [17]. In China, many salt lake brines contain a high magnesium content, resulting in a high Mg/Li ratio. Due to the similar chemical properties of lithium and magnesium, it is difficult to separate Li and Mg during extraction process of lithium [15]. Until now, many solutions are proposed for extracting Li from high-Mg/Li-ratio salt lake brine as raw materials: solvent extraction, electrodialysis, nanofiltration membrane filtration, ion exchange and adsorption [18–20]. Although the removal rate of Mg^{2+} in other studies is more than 90% and the Mg/Li ratio is as low as 0.02 [15,19,20], however, high-end technology fields such as aerospace, batteries, and medicine have very high requirements on the purity and morphology of Li_2CO_3 products. Even the low content of Mg^{2+} still has a serious impact on the high quality of crystals. Therefore, it is of great significance to study the influence of Mg^{2+} on Li_2CO_3 crystals under low Mg/Li ratio.

The complexity of ions in the solution can change the supersaturation of the mineral phase. Because of the presence of impurity ions, the solubility of the substance may change due to salting-out or chemical interaction, and the supersaturation of the solution will increase [21,22], which indicates that Li_2CO_3 crystals are more likely to combine with impurity ions, causing defects in crystalline structure and affecting crystal quality of the crystals. King et al. [13] studied the influence of Mg^{2+} on the growth of Li_2CO_3 under low Mg conditions, and the results showed that the presence of Mg^{2+} would reduce the carbonate activity and the supersaturation of the system relative to the Li_2CO_3 phase.

This study investigated the influence of Mg^{2+} on Li_2CO_3 crystallisation under different Mg/Li ratios in the Na^+, Li^+, $CO_3^{2-}//H_2O$ crystallisation system. In the analysis of combining experiment and theoretical calculation methods, the influence of different formulations of Mg^{2+} was examined in terms of purity, particle size, morphology and electronic properties of Li_2CO_3. Simultaneously, studied the doping and adsorption mechanism of Mg atom in Li_2CO_3 crystals based on the density functional theory, analysed the effect of Mg^{2+} impurity in Na^+, Li^+, $CO_3^{2-}//H_2O$ crystallisation system, and established the governing equation between Mg^{2+} content with the specific surface area. The research results have provided significant theoretical guidance for predicting the particle size distribution trend, and purity of Li_2CO_3 crystals.

2. Experiment

2.1. Materials

Lithium chloride (LiCl), sodium carbonate (Na_2CO_3), magnesium chloride ($MgCl_2$), the chemical reagents are of analytical grade, and were used without further purification. A water purification system (UPT-II-20T, Chengdu Ultrapure Technology Co., Ltd., China) was used to prepare deionized water (with a resistivity of 18.25 mω cm).

2.2. Research background

The raw materials used in this study are from a sodium sulfate subtype salt lake in Tibet, and the composition is shown in Table 1. The brine undergoes natural evaporation to enrich Li^+ into the liquid phase at a high concentration, the composition is shown in Table 2. The natural evaporation process described by the 25°C Na^+, K^+, $Li^+//Cl^-$, SO_4^{2-}–H_2O phase diagram for this brine is shown in Fig. 1, A1 represents the original halogen, and A2 represents the Li-rich brine. The saturation concentration of Li^+ in the Li-rich brine after deep removal of impurities is 4.73 mol/L, the composition is shown in Table 3. Because in the crystallisation process of Li_2CO_3, the Mg/Li ratio has a serious impact on the morphology, particle size and quality of Li_2CO_3 crystals. Therefore, this paper uses the Li^+ solution with a concentration of 4.73 mol/L as the background to study the influence of Mg^{2+} on the Li migration process in the range of Mg/Li ratio from 0.02 to 0.45.

Table 1
Chemical composition of original brine

Composition	Content (mol/L)
K^+	0.07
Mg^{2+}	0.03
Li^+	0.04
Na^+	0.81
Cl^-	0.37
SO_4^{2-}	0.23
CO_3^{2-}	0.02
B^{3+}	0.08

Table 2
Chemical composition of the system

Composition	Content (mol/L)
K^+	1.38
Mg^{2+}	2.35
Na^+	0.43
Li^+	3.66
Cl^-	21.89
SO_4^{2-}	0.52
CO_3^{2-}	2.02
H_2O	67.80

2.3. Reactive crystallisation experiments

The reaction raw materials are about 4.69 mol/L LiCl solution and 2.70 mol/L Na_2CO_3 solution, mixed with Mg-containing solution according to different Mg/Li ratios to obtain Li_2CO_3 precipitation; subsequently, the obtained crystals are characterised and analysed. A certain amount of mother liquor was added, which is the saturated solution obtained by the reaction of 4.69 mol/L LiCl solution and 2.70 mol/L Na_2CO_3 solution, and added 0.05 g seed crystals into the crystalliser, then mixed at 700 rpm in the water bath at 80°C. Mixed different concentrations of Mg-containing solution and LiCl solution respectively, used a peristaltic pump to add the Na_2CO_3 solution and the Li-containing mixed solution to the mother liquor at the speeds of 3.5 and 6 mL/min, respectively, for stirring reaction, and the stirring paddle is located in the middle of the guide tube. The device diagram is shown in Fig. 2. During the Li_2CO_3 crystallisation process, the resulting solids were labelled S0, S1, S2, S3, S4, and the reaction conditions in the Li_2CO_3 crystallisation system are shown in Table 4.

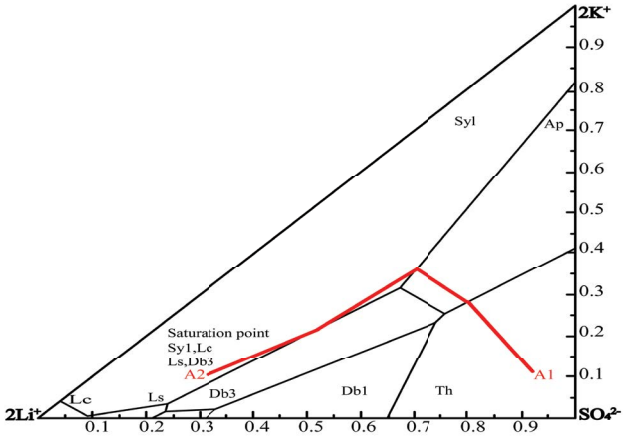

Fig. 1. Phase diagram of 25°C Na^+, K^+, $Li^+//Cl^-$, SO_4^{2-}–H_2O and isothermal evaporation route: A1, the original halogen; A2, the Li-rich brine.

Table 3
Composition of the system

Composition	Content (mol/L)
Li^+	4.73
Cl^-	4.66
Na^+	4.91
CO_3^{2-}	2.71
Mg^{2+}	0.09~2.13
H_2O	33.33

2.4. Characterisation

The Li_2CO_3 crystal was washed and dried, and the sample was analyzed using X-ray diffractometer (XRD) (X'Pert PRO). Inductively coupled plasma emission spectrometer (ICP-OES) (Thermo ICP 6500 DUO) was used to determine the content of trace elements in the solid phase products. The crystal size distribution and crystal morphology were observed and analysed by Malvern laser particle size analyser (MS 3000) and scanning electron microscope (SEM) (Hitachi SU8010). X-ray photoelectron spectroscopy (XPS) (Thermo Scientific K-Alpha) was used in a full-spectrum scan of 100 eV with a step length of 1 eV to analyse the chemical composition and atomic content of the solid surface. The crystal's specific surface area was analysed by the automatic specific surface and pore size distribution analyser (Autosorb-iQ). Energy spectroscopy (EDS) analyzes whether there is adsorption and inclusion of impurity ions in the part of the crystal.

Table 4
The chemical composition in the Li_2CO_3 crystallisation system

Experimental composition	No.				
	S0	S1	S2	S3	S4
LiCl (mol/L)	4.67	4.69	4.68	4.69	4.68
Na_2CO_3 (mol/L)	2.60	2.60	2.60	2.70	2.70
Li^+ (%)	0.53	0.51	0.51	0.52	0.51
Mg^{2+} (%)	0	0.01	0.05	0.1	0.21
Mg/Li	0	0.02	0.1	0.2	0.4

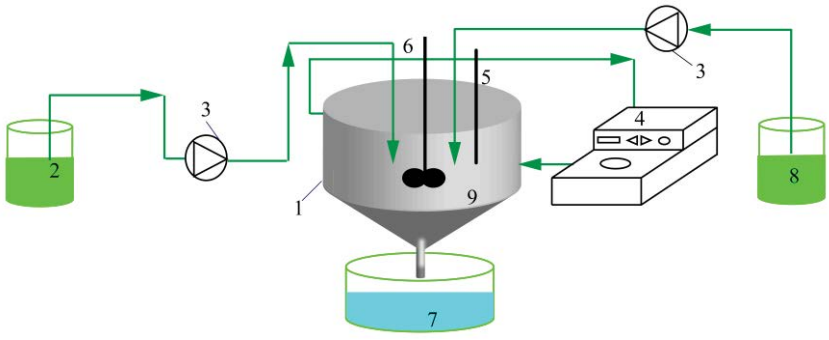

Fig. 2. Diagram of experimental setup. 1-crystalliser; 2-Na_2CO_3 solution; 3-peristaltic pump; 4-temperature water bath; 5-thermometer; 6-stirring paddle; 7-Li_2CO_3 crystal; 8-LiCl and Mg-containing mixed solution; 9-mother liquor and seed crystals.

2.5. Computational models and methods

The ideal Li_2CO_3 crystal is a monoclinic system (space group C2/c). To obtain a better Li_2CO_3 crystalline structure and calculation accuracy, the structure of the Li_2CO_3 crystal unit cell is optimised, and the optimised lattice constant is defined as a = 8.317 Å, b = 4.957 Å, c = 6.046 Å, and β = 114.617°. The optimised lattice parameters of pure Li_2CO_3 are similar to the reported values [23,24], which indicate that the model in this study is stable and reliable, and meets the requirements for calculation accuracy. The unit cell configuration of Li_2CO_3 crystal is shown in Fig. 3.

In the calculation and simulation process, the size of the unit cell has little effect on the electronic properties [25]; the Li_2CO_3 primitive cell was expanded by 2 × 3 × 2 to study the action behaviour of Mg atom in Li_2CO_3 crystals, and the supercell has a total of 288 atoms, including 96 Li atoms, 144 O atoms and 48 C atoms. Based on the density functional theory (DFT), the first-principles pseudopotential method is adopted, and crystal periodic calculation was realised in the Vienna Ab-initio Simulation Package (VASP). The VASP program calculates the lowest energy configuration of the material by minimising the structural energy of atomic reorganisation, motion and rotation [13,26]. In the calculation process, the plane wave displays the cut-off energy of the Mg-doped Li_2CO_3 crystal, which is set to 400 eV, and the sampling grid parameter of the K-point Brillouin zone is 1 × 2 × 2. The valence electrons and their orbitals involved in the calculation are as follows: Li: $2s^1$; O: $2s^22p^4$; C: $2s^22p^2$; Mg: $3s^2$. The difficulty and stability of the formation of material defects can be judged by the defect-formation energy, which can be calculated to determine whether the doping system is stable enough and the precise structure can be achieved during the experiments [27].

Defect-formation energy is a function of Fermi level and chemical potential. In the Li_2CO_3 crystal, the defect-formation energy of replacing Li atom by Mg atom is shown in Eq. (1) [28,29].

$$\Delta H = E(D) - E(\text{pure}) - \mu_i + \mu_{Li} \tag{1}$$

where $E(D)$ refers to the total energy of the system containing defect D; E(pure) refers to the total energy of the complete unit cell system; μ_i and μ_{Li} represent the chemical potential of impurity atoms and Li atoms, respectively.

The formation energy of defects in the interstitial positions of Mg atoms in Li_2CO_3 crystals is shown in Eq. (2) [28,29].

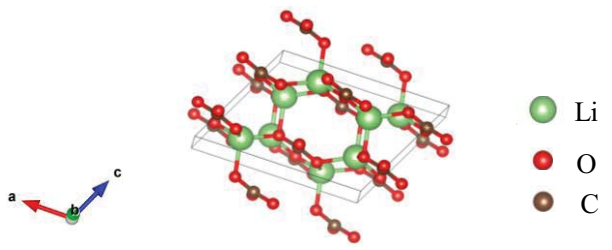

Fig. 3. Protocell structure of Li_2CO_3 crystal.

$$\Delta H = E(D,q) - E(\text{pure}) - \mu_i + q(E_{VBM} + E_F) \tag{2}$$

where $E(D,q)$ refers to the total energy of the system with defect D in the charge state q; E(pure) refers to the total energy of the complete unit cell system; E_{VBM} refers to energy at the top of the valence band of the defect-free system; E_F refers to the Fermi energy; μ_i represents the chemical potential of impurity atoms.

The chemical potential of Mg atom in a Mg-rich environment is

$$\mu_{Mg} \le E(\text{Mg}) \tag{3}$$

The chemical potential of Mg atom in a Mg-poor environment is

$$\mu_{Mg} \ge \left[E(MgCO_3) - E(CO_2) - \frac{1}{2}E(O_2) \right] \tag{4}$$

where E represents the energy of each bulk material and gas. The Mg-rich and Mg-poor limits refer to the conditions with the highest and lowest potassium chemical potentials, respectively.

By calculating the behaviour of Mg atom on the surface of Li_2CO_3 crystals, the adsorption strength of impurity ions on the crystal surface are investigated. The crystal surface model is constructed through Li_2CO_3 supercells, the surface atoms are relaxed, and the underlying atoms are fixed. To ensure that it is not affected by the interaction between molecular layers, a vacuum layer with a thickness of 15 Å is introduced in the Z-direction, and the adsorption energy [30] is defined as shown in Eq. (5).

$$E_{ads} = E_{surface+absorbate} - (E_{surface} + E_{absorbate}) \tag{5}$$

where E_{ads} refers to the adsorption energy; $E_{surface+absorbate}$ refers to the total energy of system with the adsorbed substance on the surface of the crystal; $E_{surface}$ refers to the energy of the crystal surface; $E_{absorbate}$ refers to the energy of the adsorbed substance. According to this definition, a negative value of the adsorption energy would indicate an exothermic process and thus a favourable adsorption process, whereas a positive value would indicate an endothermic and thus an unfavourable adsorption process [13].

3. Results and discussion

3.1. Influence of Mg^{2+} on Li_2CO_3 crystal morphology

Impurity ions can have a great impact on the morphology of inorganic salt crystals, when the nature of impurities is similar to the nature of crystalline ions, impurity ions can directly replace primary ions in the crystal lattice and change the crystalline nature [31]. Mg^{2+} was mixed with different Mg/Li ratios in the Li_2CO_3 crystallisation process. The resulting samples were scanned via electron microscopy, and particle size analysis was performed to study the influence of different formulations of Mg^{2+} on the morphology

and particle size of Li_2CO_3 crystals. The electron micrograph is shown in Fig. 4. The Li_2CO_3 crystals without Mg^{2+} are prismatic and have a smooth surface, when compared with the morphology of the undoped crystal, the doping of Mg^{2+} has a significant effect on the morphology of Li_2CO_3 crystals, and the crystal defects are obvious. As the Mg/Li ratio in the range 0.1–0.2 is analysed in the crystallisation system, there are flocculent and white crystals on the surface of the crystals formed by the reaction, and the crystalline surface has a rougher structural appearance. When the Mg/Li ratio is 0.4, Li_2CO_3 crystals develop from columnar to multi-layered petals, which due to the adsorption of Mg^{2+} on a certain surface of the crystal in the crystallisation system to cause the crystal to grow directionally along a specific crystal surface [14], this growth occurs simultaneously as the lamella petal crystals agglomerate.

During the crystal growth process, the presence of impurity ions have a significant impact on the nucleation and growth process of the crystal crystallisation process, which in turn affects the crystal size and particle size distribution [31]. After mixing different contents of Mg^{2+} in the Li_2CO_3 crystallisation process, the particle size of the Li_2CO_3 crystal changes significantly. The particle size analysis of the sample is shown in Fig. 5. As the content of Mg^{2+} increased, the average crystal size gradually decreases, and the crystal size distribution became uneven.

The Mg-containing solution was mixed with different Mg/Li ratios in the Li_2CO_3 crystallisation system; the solid samples were tested for purity and specific surface area. The results are shown in Table 5, and Fig. 6. As the Mg/Li ratio increased in the system, the element content data in the resulting solid samples after the second washing with 80°C hot water indicates that Mg^{2+} in Li_2CO_3 crystals is difficult to remove by washing compared with Na^+, it may be embedded in the crystal as inclusions. When the Mg/Li ratio was 0.02–0.1, the resulting samples had a smaller specific surface area compared with pure Li_2CO_3 crystals, yielding a value closer to that of pure Li_2CO_3. As the Mg/Li ratio increased to 0.2–0.4, the specific surface area increased greatly. Thus, when more Mg^{2+} content is present in the system, it is easier to increase the specific surface area of the crystal to adsorb impurity ions.

As shown in Fig. 6, the specific surface area of the sample increases linearly with an increase in the Mg^{2+} content, and the correlation equation between the Mg^{2+} content

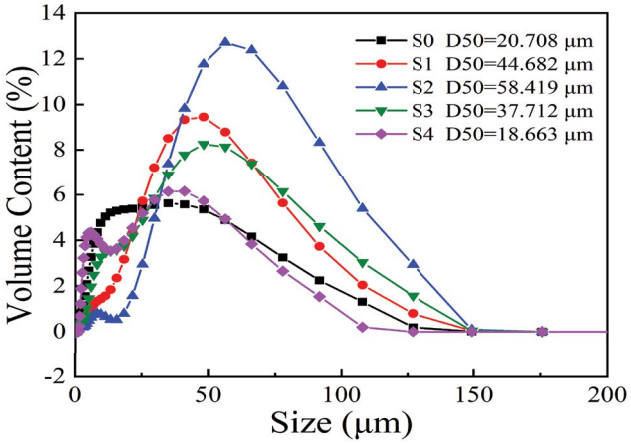

Fig. 5. The particle size distribution curve of samples under different Mg/Li ratios.

Table 5
Chemical composition of the sample under different Mg/Li ratios

Chemical composition		No.				
		S0	S1	S2	S3	S4
Content (%)	Li	18.95	17.80	17.48	16.93	14.18
	Mg	0	0.08	0.47	1.51	5.76
	Na	0	0.37	0.24	0.24	0.34

Fig. 4. SEM images of samples under different Mg/Li ratios.

and the specific surface area in the sample is obtained by linear fitting as shown in Eq. (6).

$$y = 2.2469 + 0.9446x \quad (6)$$

where, y refers to the specific surface area of Li_2CO_3 crystals, and x refers to the Mg^{2+} content in Li_2CO_3 crystals. This control equation has a strong significance for theoretically guiding the study of the effects of impurity in the crystallisation process of Li_2CO_3 in salt lake brine.

As shown in Fig. 6, the Mg^{2+} content and purity in the sample show a linearly decreasing trend. Due to the similar chemical properties of Mg and Li, it's easy for Mg^{2+} to compete with Li^+ for carbonate sites and thus to limit the growth of Li_2CO_3 [13,15], resulting in a large degree of influence on the purity of Li_2CO_3.

To analyse the mechanism of the influence of Mg^{2+} on Li_2CO_3 crystals in depth, this study analysed the samples by XPS. The Li_2CO_3 samples under different Mg/Li ratio conditions were analysed by XPS method, as shown in Fig. 7. Fig. 7a is the full spectrum of XPS, it can be seen from the figure that the sample composition mainly includes C, O, Li, among them, the Li 1s peak is located at about 55 eV, which is basically consistent with the Li 1s peak of Li_2CO_3 crystal measured in the previous study at 55.12 eV [32]. With the increase of Mg/Li ratio, the Mg 1s peak appears around 1,304 eV and the intensity gradually strengthens. The data in Table 6 shows that the atomic percentage of Mg on the crystal surface also gradually increases. This result indicates that Mg^{2+} has been incorporated into Li_2CO_3 crystals.

Take the Li_2CO_3 crystal formed by the reaction crystallization when Mg/Li ratio is 0.4 as an example, use energy spectroscopy (EDS) to analyze the micro-area element content of the generated particles and the results are shown in Fig. 8. Taking Area 1, Area 2, and Area 3 as the scanning planes of the energy spectrum respectively, it can be seen from the figure that Mg^{2+} is easy to adhere to the crystal surface, the peak and area corresponding to Mg^{2+} at Area 1 are larger than those at Area 2 and Area 3, and the crystal damage is more serious, indicating that the enrichment of Mg^{2+} at Area1 leads to more obvious defects in the crystal.

The XRD patterns of the samples obtained under different Mg/Li conditions are shown in Fig. 9. The XRD diffraction peak of the undoped sample is basically consistent with the standard pattern of Li_2CO_3 [33], and the diffraction peak is sharp, indicating that the product has good crystallinity. Therefore, it was confirmed that the sample obtained by reaction crystallisation in the undoped system is Li_2CO_3 crystal. When the Mg/Li ratio was 0.02–0.2, the XRD spectrum of the samples doped with Mg^{2+} show that

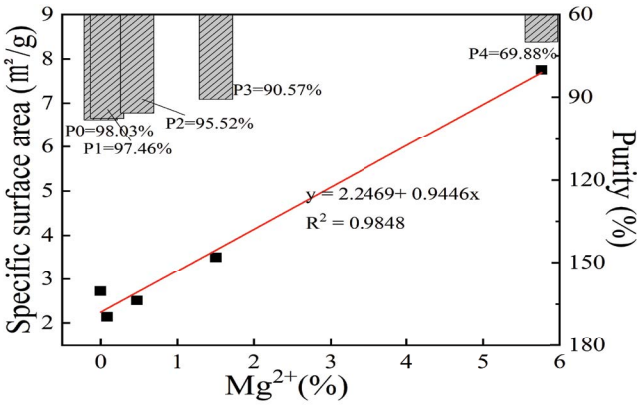

Fig. 6. Specific surface area and purity of samples with different Mg^{2+} content.

Table 6
XPS Mg 1s atomic percentage of samples under different Mg/Li ratios

No.	B.E. (eV)	Atomic (%)
S1	1,304.04	0.38
S2	1,303.99	1.65
S3	1,304.03	2.77
S4	1,303.83	5.30

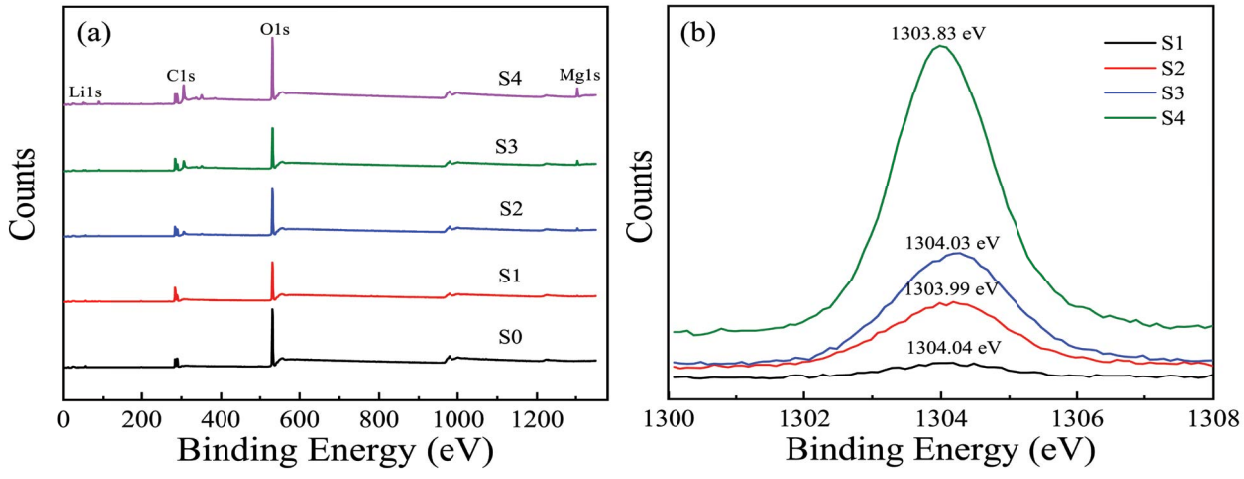

Fig. 7. XPS spectra of samples under different Mg/Li ratios: (a) full spectrum and (b) Mg 1s spectrum.

the diffraction peak of the sample is basically similar to the undoped Li_2CO_3, and there is no impurity peak. This result indicates that the addition of Mg^{2+} does not change the structure of Li_2CO_3 crystal, and the interaction between Mg^{2+} and crystal surface is mainly a surface phenomenon [33].

As the Mg/Li increases to 0.4, the intensity of diffraction peaks of (001), (110), (20–2), (31–1) and other faces of Li_2CO_3 crystals decrease. There is an impurity peak at D in Fig. 9, and its diffraction peak intensity is weak because after the small amount of CO_3^{2-} is added in the reaction process, Mg^{2+} in the system exists in the form of $MgCO_3$ firstly. When the amount of CO_3^{2-} added increases, this effect leads to an increase in pH in the solution environment; additionally, a small amount of $Mg(OH)_2$ is gradually generated. Due to the complete precipitation of $Mg(OH)_2$, the pH range is 9.4 ~ 12.4. Other studies have shown that when the pH is 10, the crystallisation effect is optimal [34]. The pH range in this reaction system is 8 ~ 9 (as shown in Table 7). Hence, the pH conditions of the liquid phase cannot meet the conditions for complete precipitation of $Mg(OH)_2$ which shows that Mg^{2+} in the system mainly exists in the form of $MgCO_3$.

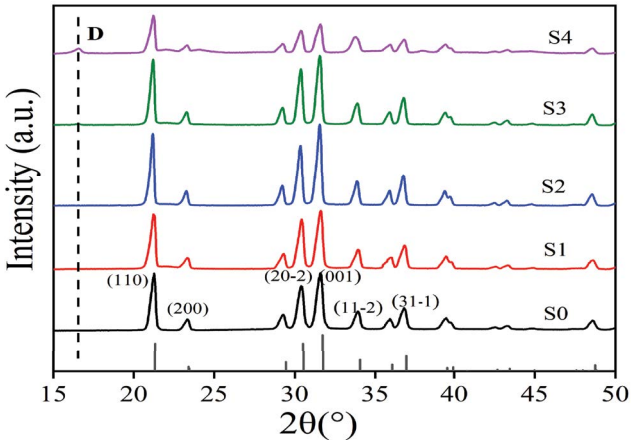

Fig. 9. XRD patterns of samples under different Mg/Li ratios.

Table 7
Liquid pH after reaction under different Mg/Li conditions

No.	pH
L1	8.75
L2	8.93
L3	8.88
L4	9.08

3.2. *Calculation and simulation study of Mg atom doping and adsorption in Li_2CO_3 crystals*

Experimental research results show that Mg^{2+} mainly affects the morphology of Li_2CO_3 crystals in the form of

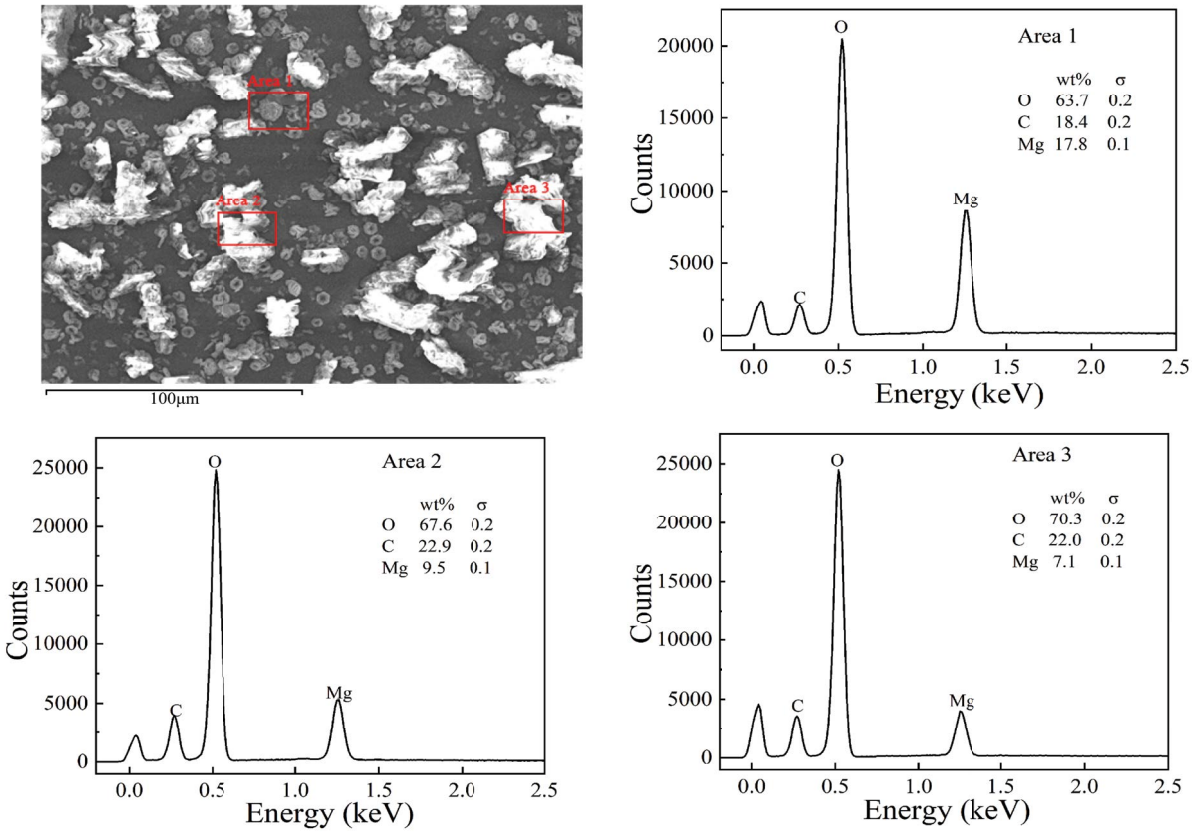

Fig. 8. Energy spectrum of Li_2CO_3 in the presence of Mg^{2+}.

inclusions and adsorption. Through theoretical calculations to study the doping and adsorption mechanism of Mg atom in Li_2CO_3 crystals furtherly, the stability of the doping of impurities into the crystal and the influence on the electronic structure of the crystal are sudied, also analyzing the form of existence and valence of Mg atoms in Li_2CO_3 crystals, revealing the interaction mechanism between Mg atoms and Li_2CO_3 crystals from the atomic level. Considering that the interaction between doped ions would affect the calculation results, this study considers doping only one impurity ion in a supercell to weaken the interaction between impurity ions [27,35]. The supercell models of the optimised Mg-doped Li_2CO_3 crystal are shown in Fig. 10.

The valence form of Mg atom in the interstitial sites of Li_2CO_3 crystals and the defect formation energy of Mg atom replacing Li atoms are calculated; the lower the defect formation energy, the smaller the amount of energy required for the formation of crystal defects. It is well known that it is easier for impurity ions to cause crystal defects in the system [36]. The curve in Fig. 11 shows the correlation between the defect formation energy of doped Li_2CO_3 crystals and the Fermi level. It can be seen from Fig. 11 that under the Mg-poor conditions, the defect formation energy of Mg_{Li} is the lowest, and signifies that Mg atom is easier to replace the position of Li atom in the crystal; under the conditions of Mg-rich and Mg-poor, the defect formation energy of $[Mg_i]^0$ is higher than $[Mg_i]^{+2}$, indicating that Mg atom mainly exists in the form of +2 valence in the crystal gap. Under the condition of Mg-rich, the defect formation energy of $[Mg_i]^{+2}$ is the lowest, it shows that Mg atom mainly exists in the interstitial sites of Li_2CO_3 crystals in the form of +2 valence, which is consistent with the conclusion that Mg^{2+} mainly exists in the form of $MgCO_3$ in the previous experimental results.

Considering the behavioral action of Mg atom on the surface of Li_2CO_3 and taking the (001) surface as an example to study, the adsorption energy of Mg atom on the Li_2CO_3 (001) surface above O, above C, and above the C–O vacancy was calculated. Fig. 12 shows the crystalline structure of Mg atom adsorbed on the (001) surface of the Li_2CO_3 crystal. The calculation results show that the adsorption energy of Magnesium atom above the C–O vacancy on the (001) surface is more negative, which indicates that the adsorption strength of Mg atom above the C–O is stronger.

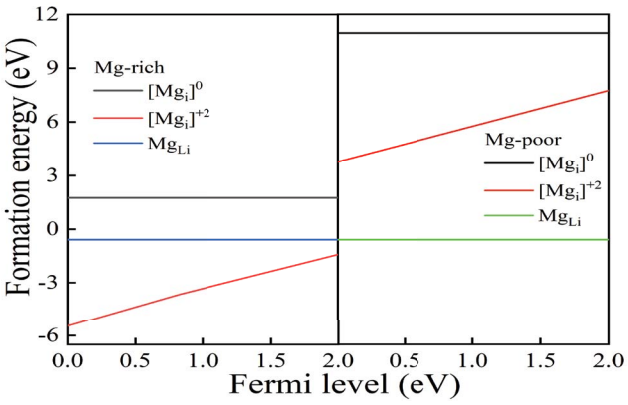

Fig. 11. Function curve of defect formation energy of doped Li_2CO_3 crystal with Fermi level.

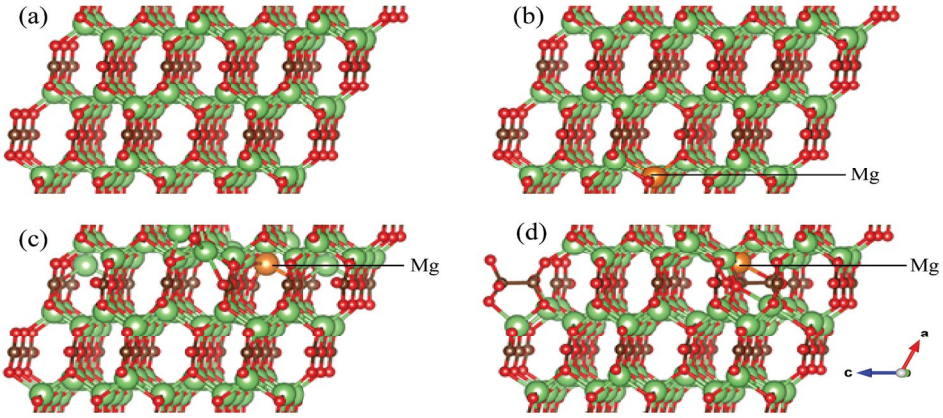

Fig. 10. Supercell model of Mg atom doped Li_2CO_3 crystal: (a) pure Li_2CO_3, (b) Mg_{Li}, (c) $[Mg_i]^{+2}$ and (d) $[Mg_i]^0$.

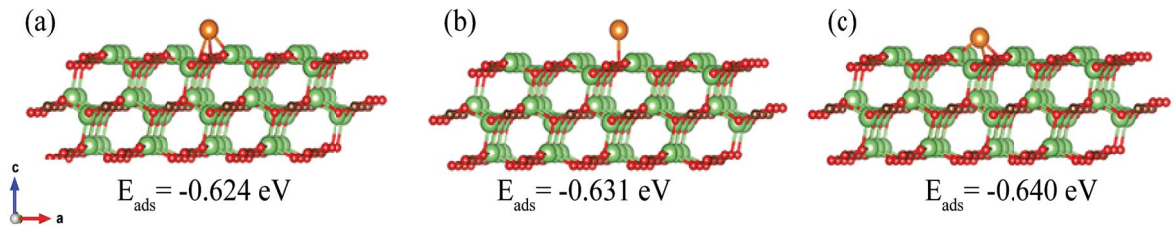

Fig. 12. The crystal structure of Mg atom adsorbed on the Li_2CO_3 (001) surface: (a) above C, (b) above O, and (c) above C–O vacancy.

The formation energy of Mg atom doped in Li_2CO_3 crystal in different forms are shown in Fig. 13. The lower the formation energy, the easier the formation of crystal defects. The formation energy of Mg atoms adsorbed on the (001) surface of the crystal, which the formation energy of defects lower than the replacement and interstitial sites, the formation energy is –5.742 eV, indicating that Mg atoms have stronger adsorption effect on the crystal surface, which is consistent with the results of Mg^{2+} mainly adsorbed on the crystal surface in the previous experiment.

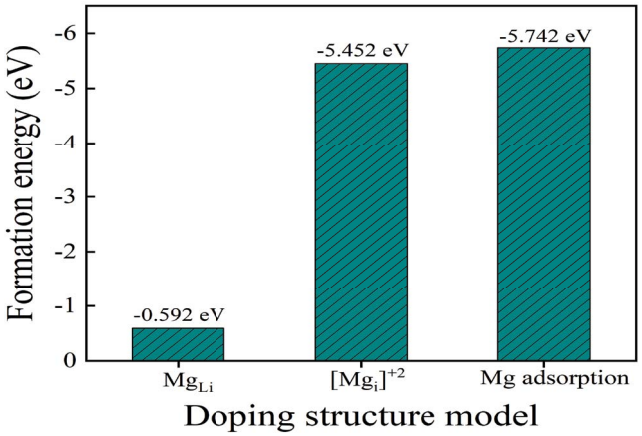

Fig. 13. Formation energy of different doping structure models.

In order to further understand the influence of Mg atom doping on the electronic structure of Li_2CO_3 crystals, the density of states of Mg atom doped Li_2CO_3 crystals is calculated and studied, where the value of Fermi level is set to 0 eV, as shown in Fig. 14. The density of states of pure Li_2CO_3 crystal symmetrical up and down are illustrated, indicating that Li_2CO_3 is a non-magnetic insulator [13]. For the symmetrical spin-up and spin-down density of states distribution, it shows that the electrons in Li_2CO_3 crystals all exist in pairs [37]. Fig. 14a shows the density of states of pure Li_2CO_3 crystals, where the band gap near the Fermi level of the total density of states is 5.06 eV. It can be seen from the information in the figure that there are partial density peaks of Li, O, and C atoms in the range of –25~15 eV and –10~–5 eV, and there is orbital hybridisation in this interval.

After Mg atom doped into Li_2CO_3 crystals, new impurity levels are generated as shown in the density of states diagram. In addition, the doping of impurity ions produces perturbation on the partial state density of atoms that play a leading role compared with the pure state density, which causes the incorporation of Mg atoms to increase or decrease the partial density peaks of some atoms near the Fermi level, the peak of the total density of states is relatively enhanced. As shown in Fig. 14b and d, the density of states on the surface of Mg atom replacing Li atom and adsorbing Li_2CO_3 shifts to a lower energy level, and the negative displacement of Mg replacing Li atoms is

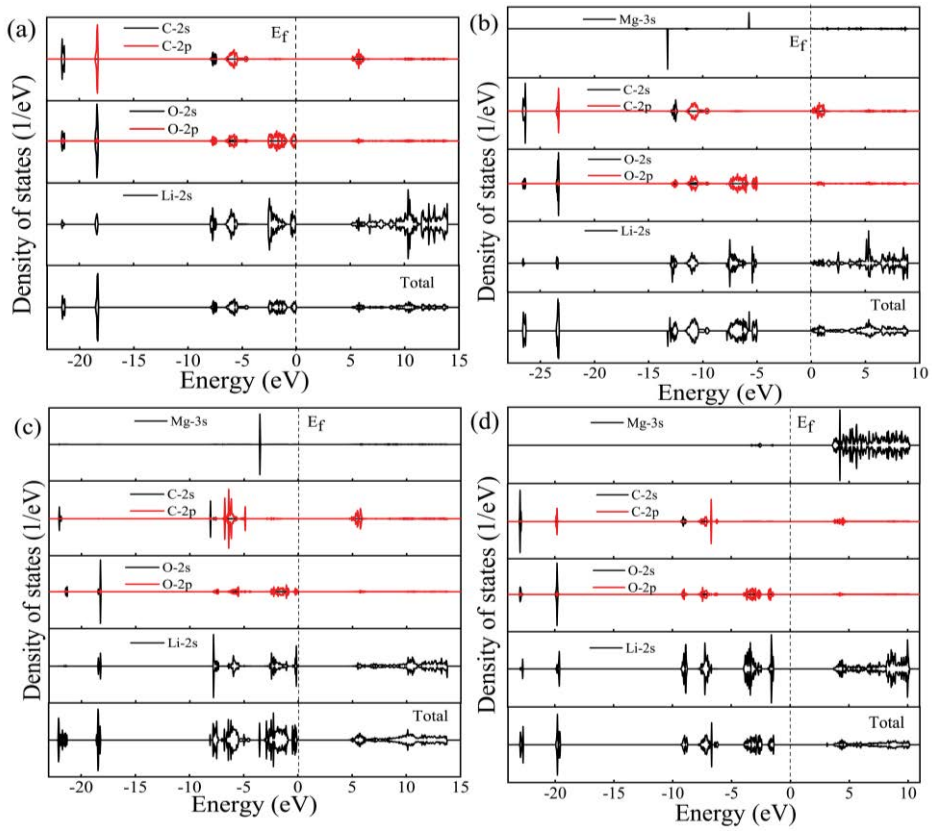

Fig. 14. Density of states of Mg atom doped Li_2CO_3 crystal: (a) pure Li_2CO_3, (b) Mg_{Li}, (c) $[Mg_i]^{+2}$, and (d) Mg is adsorbed on Li_2CO_3 (001) surface.

more obvious. As shown in Fig. 14c, when the Mg atom is in the interstitial position, the contribution of the impurity level near the Fermi level is little. The electron activity near the Fermi level is stronger and the energy is higher, and the important physical and chemical reactions always occur near the Fermi level [38,39], Mg atom doping into Li_2CO_3 crystals contributes to the Mg atomic orbitals near the Fermi level, especially when the crystal (001) surface is adsorbed, the Mg atomic orbital contribution is dominant in the conduction band, indicating that the electronic activity of Mg atoms is stronger here, resulting in it is easy to participate reactions in Li_2CO_3 crystals.

4. Conclusion

The particle size, morphology, and purity of Li_2CO_3 crystal with different Mg^{2+} content were comprehensively analysed by adding solution containing magnesium that was mixed with different Mg/Li ratios in the reaction crystallisation process of Li_2CO_3, also combined with theoretical calculations to study the doping and adsorption mechanism and stability of Mg atom in crystals, the conclusions are as follows:

- In the Na^+, Li^+, CO_3^{2-}//H_2O system, after doping with Mg^{2+}, the impurity ions mainly cover the crystalline surface in the form of $MgCO_3$ or exist as inclusions in the Li_2CO_3 crystals.
- When Mg^{2+} exists in ppm in the crystallisation system, the purity and particle size distribution of Li_2CO_3 crystals are still significantly affected. When the Mg/Li ratio is as low as 0.02, the Li_2CO_3 crystal has a purity of only 97.46%. Upon review of the data analysis and trends of the crystal's specific surface area, which increases linearly with greater content of Mg^{2+}, the governing equation is obtained: $y = 2.2469 + 0.9446x$.
- The doping and adsorption mechanism of Mg atom in the Li_2CO_3 crystal was analysed deeply by computational simulation. Mg atoms mainly exist in Li_2CO_3 crystals in the form of +2 valence. Combined with the comparative analysis of defect formation energy and density of states, the formation energy of Mg atom adsorbed on the crystal surface is the lowest, and the electronic activity of impurity atoms is stronger, which is consistent with the previous experimental results.

Symbols

ΔH	—	Defect-formation energy, eV
$E(D)$	—	Total energy of the system containing defect D, eV
E(pure)	—	Total energy of the complete unit cell system, eV
μ_i	—	Chemical potential of impurity atoms
μ_{Li}	—	Chemical potential of Li atoms
$E(D,q)$	—	Total energy of the system with defect D in the charge state q, eV
E_{VBM}	—	Energy at the top of the valence band of the defect-free system, eV
E_F	—	Fermi energy, eV
E	—	Energy of each bulk material and gas, eV
E_{ads}	—	Adsorption energy, eV
$E_{surface+absorbate}$	—	Total energy of system with the adsorbed substance on the surface of the crystal, eV
$E_{surface}$	—	Energy of the crystal surface, eV
$E_{absorbate}$	—	Energy of the adsorbed substance, eV
y	—	Specific surface area of Li_2CO_3 crystals, m^2/g
x	—	Mg^{2+} content in Li_2CO_3 crystals

References

[1] J.W. Fergus, Recent developments in cathode materials for lithium ion batteries, J. Power Sources, 195 (2010) 939–954.
[2] W.C. Yang, L. Zhou, J.Y. Dai, L.N. Zhou, M.J. Zhang, C. Xie, H.X. Hao, B.H. Hou, Y. Bao, Q.X. Ying, Crystallization of lithium carbonate from aqueous solution: new insights into crystal agglomeration, Ind. Eng. Chem. Res., 58 (2019) 18448–18455.
[3] D.Z. Lin, Use of lithium and its resource exploitation, China Saf. Sci. J., 14 (2004) 72–76.
[4] Q.Z. You, Application of lithium in glass ceramic industry, Word Nonferrous Met., 2 (2000) 26–31.
[5] M.A. Delgado, C. Valencia, M.C. Sánchez, J.M. Franco, C. Gallegos, Thermorheological behaviour of a lithium lubricating grease, Tribology Lett., 23 (2006) 47–54.
[6] V. Etacheri, R. Marom, R. Elazari, G. Salitra, D. Aurbach, Challenges in the development of advanced Li-ion batteries: a review, Energy Environ. Sci., 4 (2011) 3243–3262.
[7] W.G. Paul, A.M. Pablo, A.K. Gregory, E.K. Stephen, P.M. Everson, J.W. Timothy, Global lithium availability: a constraint for electric vehicles, J. Ind. Ecol., 15 (2011) 760–775.
[8] U. Bardi, Extracting minerals from seawater: an energy analysis, Sustainability, 2 (2010) 980–992.
[9] P.C. Lu, X.F. Song, H. Chen, Y.Z. Sun, J.G. Yu, The effect of boron forms on the crystallization process of lithium carbonate, Cryst. Res. Technol., 55 (2019) 1–9.
[10] Y. Pranolo, Z.W. Zhu, C.Y. Cheng, Separation of lithium from sodium in chloride solutions using SSX systems with LIX 54 and Cyanex 923, Hydrometallurgy, 154 (2015) 33–39.
[11] W.P. Liu, H. Xu, X.C. Shi, X.Y. Yang, Fractional crystallization for extracting lithium from Cha'erhan tail brine, Hydrometallurgy, 167 (2017) 124–128.
[12] H. Chen, S.J. Duan, Y.Z. Sun, X.F. Song, J.G. Yu, Molecular dynamics simulations of solvent effects on the crystal morphology of lithium carbonate, RSC Adv., 10 (2020) 5604–5609.
[13] H.E. King, A. Salisbury, J. Huijsmans, N.Y. Dzade, O. Plümper, Influence of inorganic solution components on lithium carbonate crystal growth, Cryst. Res. Technol., 19 (2019) 6994–7006.
[14] S.J. Duan, Multi-Scale Regulation of Reactive Crystallization of Lithium Carbonate, D. East China University of Science and Technology, 2018.
[15] H.Y. Wang, Y. Zhong, B.Q. Du, Y.J. Zhao, M. Wang, Recovery of both magnesium and lithium from high Mg/Li ratio brines using a novel process, Hydrometallurgy, 175 (2018) 102–108.
[16] N. Linneen, R. Bhavel, D. Woerner, Purification of industrial grade lithium chloride for the recovery of high purity battery grade lithium carbonate, Sep. Purif. Technol., 214 (2019) 168–173.
[17] M.-S. Yoon, M. Islam, S.-C. Ur, The role of impurities on electrochemical properties of $LiFePO_4$ cathode material, Ceram Int., 39 (2013) S647–S651.
[18] C.L. Shi, Y. Jing, J. Xiao, X.Q. Wang, Y. Yao, Y.Z. Jia, Solvent extraction of lithium from aqueous solution using non-fluorinated functionalized ionic liquids as extraction agents, Sep. Purif. Technol., 172 (2017) 473–479.
[19] Z.-Y. Ji, Q.-B. Chen, J.-S. Yuan, J. Liu, Y.-Y. Zhao, W.-X. Feng, Preliminary study on recovering lithium from high Mg^{2+}/Li^+ ratio brines by electrodialysis, Sep. Purif. Technol., 172 (2017) 168–177.

[20] Y. Li, M. Wang, Y.J. Zhao, H.Y. Wang, H.J. Yang, Z.H. Zhu, Study on separation performance of magnesium and lithium from salt lake brine with high magnesium and lithium ratio by nanofiltration membrane, J. Chem. Ind., (2020) 1–21.
[21] T.L. Ye, Principle and Application of Chemical of Crystallization Process, Beijing University of Technology press, Beijing, 2006, pp. 78–86.
[22] H.E. King, H. Satoh, K. Tsukamoto, A. Putnis, Nanoscale observations of magnesite growth in chloride- and sulfate-rich solutions, Environ. Sci. Technol., 47 (2013) 8684–8691.
[23] Y. Idemoto, J.W. Richardson Jr., N. Koura, S. Kohara, C.-K. Loong, Crystal structure of $(Li_xK_{1-x})_2CO_3$(x = 0, 0.43, 0.5, 0.62, 1) by neutron powder diffraction analysis, J. Phys. Chem. Solids, 59 (1998) 363–376.
[24] L. Pastero, F.R. Massaro, D. Aquilano, Experimental and theoretical morphology of single and twinned crystals of Li_2CO_3 (zabuyelite), Cryst. Growth Des., 7 (2007) 2749–2755.
[25] X.F. Liu, X.J. Cao, L.H. He, C. Chen, First principles study on the effect of N doping concentration on the photocatalytic activity of TiO_2, New Chem. Mater., 43 (2015) 219–222.
[26] J.J. Zhu, M. Gu, X.L. Liu, B. Liu, S.M. Huang, C. Ni, Phase transition and elastic and optical properties of Lu_2SiO_5, Opt. Mater., 35 (2013) 1659–1663.
[27] J.F. Ding, X.M. Li, L.-L. Cui, C. Cao, H.H. Wang, J. Cao, Electronic and optical properties of anion-doped c-ZrO_2 from first-principles calculations, J. Cent. South Univ., 21 (2014) 2584–2589.
[28] L.C. Jia, M. Gu, G. Song, J.J. Zhu, Stability and electronic properties of O vacancies and Ce^{4+} in Lu_2SiO_5 tuned by C doping, Opt. Mater., 93 (2019) 15–18.
[29] C.G. Van de Walle, G. Chris, First-principles calculations for defects and impurities: applications to III-nitrides, J. Appl. Phys., 95 (2004) 3851–3879.
[30] Y. Han, C.-J. Liu, Q.F. Ge, Interaction of Pt clusters with the anatase TiO_2(101) surface: a first principles study, J. Phys. Chem. B, 110 (2006) 7463–7472.
[31] H.Y. Gong, C.H. Li, P.P. Wang, H.Q. Wang, Research progress of the influence of impurity on the crystallization process of solution, Chem. Biol. Eng., 27 (2010) 9–12.
[32] X. Li, B. Yuan, M.G. Yi, Removal of trace sulfur from lithium carbonate by hydrothermal method, Inorg. Salt Ind., 51 (2019) 28–30.
[33] P. Taborga, I. Brito, T.A. Graber, Effect of additives on size and shape of lithium carbonate crystals, J. Cryst. Growth, 460 (2017) 5–12.
[34] J.-P. Hsu, A. Nacu, Preparation of submicron-sized $Mg(OH)_2$ particles through precipitation, Colloids Surf., A, 262 (2006) 220–231.
[35] H.Q. Zhu, First Principles Study on Rutile Doped TiO_2 and Its Surface Adsorbed Molecules, Chongqing Normal University, 2015.
[36] N.W. Guo, E.P. Deng, Z.B. Zhao, J. Chen, F. Yang, Y.Z. Huang, First-principles study of point defects in 4H-SiC, Semiconductor Technol., 43 (2018) 63–69.
[37] Z. Liu, J.J. Zhang, Y. Lv, X. Zhou, S.M. Li, Impact of non-metal dopants on band-gap engineering and photocatalytic ability of λ-Ta_2O_5 from a hybrid density functional study, J. Alloys Compd., 100 (2017) 1–11.
[38] G.Y. Wu, Y.G. Zhu, Z.G. Yan, G.B. Zhen, X. Tan, G.C. Liu, J. Zhang, First principles study on separation of magnesite and quartz flotation, Min. Metall., 24 (2015) 11–14.
[39] Y.M. Zhu, Y.Y. Zhang, N. Nan, R.Q. Xie, J. Liu, First principles calculation of apatite crystal and surface gene, Metal Min., 6 (2020) 87–93.